



# **The Effect of Amino Acids on the Fenton and photo-Fenton Reactions in Cloud Water: Unraveling the Dual Role of Glutamic Acid**

*Peng Cheng<sup>1,2</sup>, Gilles Mailhot<sup>1,3</sup>, Mohamed Sarakha<sup>1</sup>, Guillaume. Voyard<sup>1</sup>, Daniele Scheres Firak<sup>4</sup>, Thomas Schaefer<sup>4</sup>, Hartmut Herrmann<sup>4</sup>, Marcello Brigante<sup>1\*</sup>*

<sup>1</sup> Université Clermont Auvergne, CNRS, Institut de Chimie de Clermont-Ferrand, F-63000 Clermont-Ferrand, France.

<sup>2</sup> Department of Environmental Engineering, School of Resources and Environmental Science, Wuhan University, 430079, PR China

<sup>3</sup> Université Clermont Auvergne, CNRS, Laboratoire de Météorologie Physique (LaMP), F-63000 Clermont-Ferrand, France.

<sup>4</sup> Atmospheric Chemistry Department (ACD), Leibniz- Institute for Tropospheric Research (TROPOS), 04318 Leipzig, Germany

\*Corresponding author:

Marcello Brigante ([Marcello.Brigante@uca.fr](mailto:Marcello.Brigante@uca.fr))



19 **ABSTRACT**

20 In this work, Glutamic acid (Glu) was selected as a model amino acid (AAs) to investigate its  
21 complexation with Fe(III) and Fe(II), focusing on its impact on the Fenton reaction and the  
22 photolysis of Fe(III) in cloud aqueous phase. Glu was found to enhance the rate constant for the  
23 reaction of Fe(II)-Glu with H<sub>2</sub>O<sub>2</sub> to  $1.54 \pm 0.13 \times 10^4 \text{ M}^{-1} \text{ s}^{-1}$ , which is significantly higher than  
24 that of classic Fenton reactions ( $\sim 50\text{--}70 \text{ M}^{-1} \text{ s}^{-1}$ ). In contrast, the photolysis quantum yield of  
25 Fe(III)-Glu complex was determined to be 0.037 under solar simulated irradiation, largely lower  
26 than Fe(III)-hydroxy complexes (0.216). In the overall process (Fenton or Fe(III) photolysis),  
27 it was found that  $\bullet\text{OH}$  formation decreased in the presence of Glu. Additionally, the fate of Glu  
28 in the presence of Fe(III) was investigated as well as the oxidation process (driven by  $\bullet\text{OH}$  and  
29 ligand-to-metal charge transfer (LMCT) reaction) led to the formation of short-chain carboxylic  
30 acids and ammonium under simulated solar light. Interestingly, these two processes generated  
31 different primary short-chain carboxylic acids, indicating distinct mechanisms. This study  
32 provides valuable insights into the role and fate of amino acids in atmospheric chemistry,  
33 helping to further understand their impact on atmospheric processes.

34  
35 **KEYWORDS:** Glutamic acid, Fenton, hydroxyl radical, oxidant capacity, atmospheric  
36 composition

37  
38 **SYNOPSIS**

39 This study investigates the complexation of Fe(II) and Fe(III) with glutamic acid under cloud  
40 water conditions and the effect on Fenton and photo-Fenton reactions, hydroxyl radical  
41 formation, and their impact on amino acid oxidation.



## 42 1. INTRODUCTION

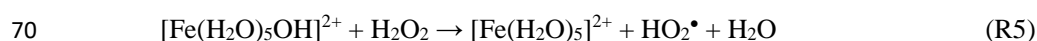
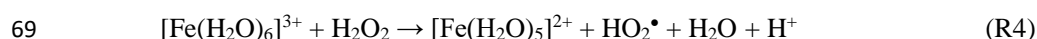
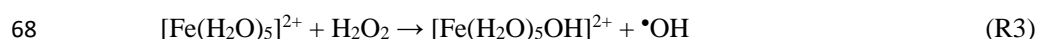
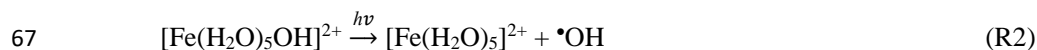
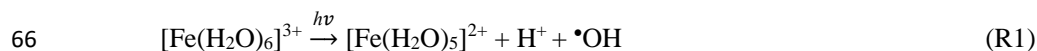
43 The Earth's atmosphere is a dynamic system in which different phases, including gases, aerosol  
44 particles, water droplets, and ice particles, are all engaged in complex chemical interactions that  
45 continually modify the atmospheric chemical composition (Bianco et al., 2020; Kanakidou et  
46 al., 2018). Among these, the cloud aqueous phase stands out as a critical reactive system,  
47 encompassing gaseous, liquid, and solid components. In recent years, intensified research  
48 efforts have centered on unraveling the composition of atmospheric cloud waters, significantly  
49 advancing our comprehension of multiphase chemistry within the atmosphere (Bianco et al.,  
50 2018). Common components identified in both aerosols and cloud water include inorganic ions,  
51 transition metal ions (TMI) (Angle et al., 2021; Bianco et al., 2017), and organic carbon  
52 (Battaglia Jr. et al., 2019).

53 Recent investigations have unveiled the presence of reactive oxygen species (ROS) in viscous  
54 aerosol particles, highlighting their pronounced reactivity in such environments (Alpert et al.,  
55 2021; Edwards et al., 2022). Hydroxy radicals ( $\bullet\text{OH}$ ) emerge as primary ROS in the atmospheric  
56 water phase, with concentrations estimated between  $10^{-14}$  to  $10^{-12} \text{ M}^{-1}$  (Bianco et al., 2020;  
57 Gligorovski et al., 2015). Key sources of  $\bullet\text{OH}$  include gas-droplet partitioning and in situ  
58 formation through processes like photolysis at surfaces or in the bulk phase, such as the  
59 photolysis of TMI and hydrogen peroxide ( $\text{H}_2\text{O}_2$ ) (Bianco et al., 2015; Tilgner et al., 2013).

60 Iron (Fe), copper (Cu), and manganese (Mn) have gained prominence as pivotal metals in  
61 atmospheric chemical processes due to their elevated concentrations, with Fe averaging around  
62  $10^{-6} \text{ M}$  in the atmospheric aqueous phase (Sorooshian et al., 2013). Experimental evidence and  
63 literature emphasize the crucial role of iron, particularly via (photo)-Fenton and (photo)-Fenton-



64 like processes, in the generation and budgeting of  $\bullet\text{OH}$  (R1-R5) (Guo et al., 2014; Tilgner et al.,  
65 2013).



71 While Fe(III)/Fe(II) ions precipitate as oxides or hydroxides at pH higher than 4.0, in the cloud  
72 water phase, iron complexes with organic ligands enhance stability under typical cloud water  
73 photooxidation conditions (Soriano-Molina et al., 2018; Yuan et al., 2020). Various organic  
74 ligands, including carboxylic acids and aldehydes, have been extensively studied (Long et al.,  
75 2013; Marion et al., 2018; Soriano-Molina et al., 2018). However, less than 30 % of the  
76 dissolved organic carbon (DOC) in the cloud-aqueous phase has been molecularly characterized,  
77 with amino acids (AAs) constituting a significant portion of DOC (Bianco et al., 2016).  
78 Numerous field studies have confirmed the presence of AA in cloud water, rain, fog, and  
79 aerosols, with concentrations typically ranging from low nanomolar to micromolar levels,  
80 depending on the location and sampling method (Matos et al., 2016; van Pinxteren et al., 2023;  
81 Renard et al., 2022; Triesch et al., 2021). For example, Renard et al. (2022) detected more than  
82 15 amino acids in cloud water collected at Puy de Dôme, France, with glutamate being one of  
83 the most abundant species. These compounds originate from both primary emissions (e.g.,  
84 bioaerosols, ocean spray) and secondary atmospheric processes (e.g., processing of proteins or  
85 peptides within clouds) (Mace et al., 2003; Samy et al., 2011). Amino acids, as key nitrogen-  
86 containing components in organic matter, can significantly affect the oxidation capacity of



cloud water through free radical scavenging and metal complexation reactions (Bianco et al., 2016; Marion et al., 2018), but their specific atmospheric reactivity and transformation mechanisms are still unclear. The photochemical behavior and fate of AAs in the atmosphere remain relatively unexplored. For example, tryptophan can undergo direct photolysis, producing low-molecular-weight compounds and dimerization products under solar-simulated conditions. Recent investigations into the fate of the Fe(III)-aspartate complex demonstrate ligand-to-metal charge transfer reactions (LMCT) and the formation of ammonia and short-chain carboxylic acids (Marion et al., 2018).

However, the effect of the complexation between Fe(II) and AAs on the rate of Fenton reaction and the yield of  $\bullet\text{OH}$  in the atmosphere has not yet been investigated. Moreover, the effect of the complexation between Fe(III) and AAs on the quantum yield of atmospheric photolysis of Fe(III) deserves further investigation, since both processes highly affect the budget of  $\bullet\text{OH}$  during the day and night in the atmosphere. In addition, the complexation between Fe(III) and AAs introduces two distinct photooxidation pathways: the photolysis of Fe-AAs complexes and reactions between AAs and (photo)-generated  $\bullet\text{OH}$ . Although both pathways significantly contribute to the transformation of AAs in cloud water and impact inorganic and organic chemical compositions, their mechanisms still lack further study, especially in terms of products generation.

This study specifically focuses on glutamic acid (Glu), an AA regularly detected in cloud water and aerosols (van Pinxteren et al., 2012; Triesch et al., 2021), and on the investigation of its impact on iron (Fe(II)/Fe(III)) reactivity. The study explored i) the effect of Glu on the rate and  $\bullet\text{OH}$  yield of the Fenton reaction; and ii) the effect of Glu on the  $\bullet\text{OH}$  production and Fe(II) quantum yield during the Fe(III) photolysis. In addition, the study explores iii) two pathways



110 of Fe(III) and Fe(III)-Glu complex photolysis: the LMCT process and the reaction between Glu  
111 and  $\bullet\text{OH}$ , assessing their respective contributions to Glu fate. Utilizing competitive kinetic  
112 experiments, the contributions of each pathway were estimated, and a detailed investigation of  
113 the formation, and chemical mechanisms of transformation products was carried out. Ultimately,  
114 our study aims to quantify the diverse contributions of different pathways in amino acid  
115 conversion in the presence of iron.

## 116 **2. MATERIAL AND METHODS**

### 117 **2.1. Chemicals**

118 All chemicals were used without further purification: Fe(III)-perchlorate (99.9 %), Fe(II)-  
119 perchlorate (99.9 %), L-glutamic acid monosodium salt (Glu, 99 %), hydrogen peroxide ( $\text{H}_2\text{O}_2$ ,  
120 30 %), malonic acid (99.0 %), and 2,4-dinitrophenylhydrazine (DNPH, 97 %) were purchase  
121 from Sigma Aldrich. Sodium formate (99.0 %), potassium oxalate monohydrate (99.0 %),  
122 sodium succinate dibasic (98.0 %), and 3-(2-pyridyl)-5,6-diphenyl-1,2,4-triazine-p, p'-sulfonic  
123 acid monosodium salt hydrate (Ferrozine, 97 %) were purchased from Fluka. Ammonium  
124 acetate (99.3 %) was purchased from Fisher. Water was purified using a reverse osmosis RIOS  
125 5 and Synergy (Millipore) device (resistivity  $18.2 \text{ M}\Omega \text{ cm}$ ,  $\text{DOC} < 0.1 \text{ mg L}^{-1}$ ). All solutions  
126 were prepared in milli-Q water.

### 127 **2.2. Experimental procedure**

#### 128 **2.2.1. Fenton reaction**

129 The Fenton experiments were carried out with Fe(II) perchlorate at room temperature and a pH  
130 of  $5.6 \pm 0.1$  (Kinetic experiments) and  $3.8 \pm 0.1$  (Electron spin resonance (ESR) experiments).  
131 The Fenton kinetic experiments were initiated by the addition of the  $\text{H}_2\text{O}_2$ . The solution was



continuously stirred during the reaction. The pH of the solution was adjusted using  $\text{HClO}_4$  or NaOH solutions. The samples were taken every 15 seconds and mixed with a solution of Ferrozine in phosphate buffer ( $\text{pH} = 7.0 \pm 0.1$ ) (Gabet et al., 2023). Phenol was used as  $\bullet\text{OH}$  scavenger in the experiment. As a scavenger, the required concentration of phenol was calculated to quench  $\bullet\text{OH}$  so that theoretically 99 % of  $\bullet\text{OH}$  can be trapped via reacting with phenol. The same method was used in the presence of Glutamic acid (Glu) to study the  $\text{Fe(II)-Glu}$  complex Fenton-like reaction at the same pH. To get different fractions of  $\text{Fe(II)-Glu}$ ,  $\text{Fe(II)}$  was mixed with varying concentrations of Glu solution (0 - 25 mM) to calculate the reactivity constant of the Fenton reaction. The experimental data were analyzed using Origin 2019 software. To determine and quantify the  $\bullet\text{OH}$  generation in the Fenton reaction, the ESR experiment was carried out using 5,5-dimethyl-1-pyrroline-N-oxide (DMPO) as the spin trap.  $\text{Fe(ClO}_4)_2$  and  $\text{H}_2\text{O}_2$  were mixed with DMPO at a pH of  $3.8 \pm 0.1$ . The pH was set because the ESR signal intensity was lower at a higher pH = 4.0. ESR spectroscopy was performed on a Bruker EMX-plus spectrometer using the resonator 4119HS. Detailed information was provided in the supplementary material section (SM1).

### 2.2.2. Photolysis of $\text{Fe(III)}$

To study the  $\text{Fe(III)}$  photolysis, isopropanol was used as a scavenger in the solution to quench the generated  $\bullet\text{OH}$  radicals. The pH of the solution was adjusted to  $3.8 \pm 0.1$  with  $\text{HClO}_4$  or NaOH solutions. The  $\text{Fe(III)}$  solution was irradiated in a Pyrex jacketed cylindrical reactor (Fig. SM1) with a circulation cooling system to keep a constant temperature of  $283 \pm 0.2$  K. The reactor was located at the focal point of a 500 W xenon lamp equipped with a Pyrex filter to remove wavelengths  $< 290$  nm and a water filter for infrared radiation absorption. The solution was stirred with a Teflon-coated magnetic stirring bar to ensure homogeneity. The same setup



155 was used for the photolysis experiments in the presence of Fe(III)-Glu complexes. Different  
156 fractions of Fe(III)-Glu were achieved by adding different amounts of a Glu 50 mM stock  
157 solution (designed [Glu] = 0 - 200  $\mu$ M).

158 The emission spectrum of the irradiation setup was recorded using a calibrated CCD camera  
159 (Ocean Optics USB 2000+UV-Vis) coupled with an optical fiber. A total Energy of  $8.38 \times 10^3$   
160  $\mu$ W cm<sup>-2</sup> s<sup>-1</sup> was determined between 290 and 500 nm (UV contribution from 290 to 400 nm)  
161 as shown in **Fig. SM2**. The Energy and photonic flux ( $I_0$ ) of the polychromatic irradiation at  
162 every nanometer wavelength are listed in **Table SM1**. Detailed information about the  
163 calculation of the Fe(III) and Fe(III)-Glu photolysis quantum yield is given in the  
164 supplementary material section (**SM2**). To quantify the  $\bullet$ OH generation during the Fe(III)  
165 photolysis, isopropanol was used in excess (10 mM) as a selective  $\bullet$ OH probe. Isopropanol  
166 reacts with  $\bullet$ OH to form acetone which was quantified by HPLC (see section 2.4) (Motohashi  
167 and Saito, 1993).

### 168 **2.2.3. Photodegradation of Glu**

169 To investigate the fate of Glu in various systems, experiments were performed using the  
170 previously described photoreactor setup. Glu solutions, either alone or mixed with Fe(III)  
171 and/or H<sub>2</sub>O<sub>2</sub>, were irradiated under simulated solar light at pH  $3.8 \pm 0.1$ . Samples were collected  
172 at specific time intervals and analyzed using HPLC-MS (see section 2.4). To calculate and  
173 compare the photodegradation kinetics of Glu in different systems, a pseudo-first-order kinetic  
174 model was applied, expressed as Equation (1):

$$175 \quad -\ln(C_t/C_0) = k_{\text{obs}} t \quad \text{Eq (1)}$$





176 where  $C_0$  represents the initial concentration of Glu, and  $C_t$  is the concentration of Glu at time  
177  $t$  of irradiation. In addition, IC-MS and TOC analyses were performed to identify the generated  
178 by-products and assess the mineralization of Glu (see section 2.4).

### 179 **2.3. Study of the speciation of the Fe(III)/Fe(II)-Glu complex**

180 The speciation of the Fe(III)/Fe(II)-Glu complex was studied using the Hyss 2009 software.  
181 This analysis included the iron, iron-aqua, iron hydroxy, and iron-Glu complexes in the solution.  
182 The parameters used in the software, such as iron and Glu concentrations, kept consistent with  
183 the one in the experimental procedure. The stability constants (log K) used for the complexes,  
184 such as the Fe(II)-Glu and Fe(III)-Glu complexes, etc. are listed in **Table SM2**. These constants  
185 are derived from the Visual MINTEQ database or NIST database 46 and have been corrected  
186 for a temperature of 25 °C and an ionic strength (I) of 0 M. The detailed method is provided in  
187 the supplementary material section (**SM3**).

### 188 **2.4. Chemical analysis**

#### 189 **2.4.1. Fe(II), H<sub>2</sub>O<sub>2</sub>, and Acetone quantification**

190 Iron (II) concentration was determined by using Ferrozine, which forms a stable magenta  
191 complex with Fe(II) (Fe(II)-ferrozine) (Gabet et al., 2023). Hydrogen peroxide concentration  
192 during experiments was determined by using a spectrofluorimetric quantification method  
193 (Bader et al., 1988). The concentration of generated acetone in the solution was evaluated by  
194 HPLC (Shimadzu NEXERA XR HPL) equipped with a photodiode array detector and an  
195 autosampler (Wang et al., 2005). **Fig. SM3** shows the calibration curve of Fe(II), H<sub>2</sub>O<sub>2</sub>, and  
196 acetone. More details are given in the supplementary material section (**SM4**).

#### 197 **2.4.2. UPLC-MS, IC-MS and TOC**



198 The quantification of Glutamic acid (Glu) and the identification of its transformation products  
199 was conducted using a ThermoScientific Orbitrap Q-Exactive high-resolution mass  
200 spectrometry (HRMS) coupled with a ThermoScientific Ultimate 3000 RSLC ultra-high-  
201 performance liquid chromatography (UPLC) system. The quantification of carboxylic acid by-  
202 products and  $\text{NH}_4^+$  resulting from Glu degradation was performed using a Thermo-Fisher  
203 Scientific ICS-6000 Ionic chromatograph interfaced with a simple quadrupole mass  
204 spectrometer (ISQ-EC-Thermo Scientific). The total organic carbon (TOC) concentration in the  
205 aqueous solution was followed by a Shimadzu TOC 5050A analyzer. Detailed information is  
206 reported in the Supplementary Material section (**SM5**).

## 207 **2.5. Kinetic Modeling**

208 To verify the obtained experimental reactivity constants of the reaction between Fe(II)-Glu and  
209  $\text{H}_2\text{O}_2$ , COPASI software was utilized to simulate the kinetics of Fe(II) consumption and  
210 generation of  $\cdot\text{OH}$  in the Fenton reaction in the presence of Glu using the default settings of the  
211 deterministic LSODA algorithm to solve ordinary differential equations (Hoops et al., 2006).  
212 The chemical reactions considered in the model are provided in **Table SM3**. The majority of  
213 rate constants used in the model were available in the literature or obtained from experimental  
214 results. For the unknown or uncertain rate constants, the value is obtained from the estimation  
215 according to a similar reaction.

## 216 **3. RESULTS AND DISCUSSION**

217 To investigate the effect of Glu on the Fe(II)/Fe(III) cycle, a complex set of experiments was  
218 performed. First, the complexation of Fe(II)/Fe(III) with Glu was studied as a function of pH  
219 and the initial concentration of Glu. Second, to study the effect of Glu on the Fenton reaction,



its rate constants and  $\bullet\text{OH}$  generation in the presence of Glu were obtained experimentally and using the kinetic model. The formation rates of Fe(II) and  $\bullet\text{OH}$  were determined from Fe(III) photolysis with or without Glu. Finally, the mechanism of Glu photo-transformation was reported.

### 3.1. Complexation of Glu with Fe(II)/Fe(III)

The Fe speciation was initially investigated to understand how Glu interacts with iron ions under various conditions with Hyss2009 software. **Fig. SM4a** shows the speciation of 20  $\mu\text{M}$  Fe(II) in the presence of Glu (0.2 – 25 mM) across a pH range of 4 to 10. It can be observed that Fe(II) predominates until pH = 5, while the fraction of the Fe(II)-Glu complex increases after this pH. Hence, a higher pH (5.6) was selected for the Fenton reaction to guarantee the presence of complex, while still working under aerosol/cloud conditions and to avoid iron precipitation occurring at higher pH values. At pH 5.6, the Fe(II)-Glu complex accounts for 2.2 % in the presence of 20  $\mu\text{M}$  Fe(II) and 25 mM Glu. The complex fractions at varying Glu concentrations at pH = 5.6 are provided in **Table SM4**.

**Fig. SM4b** shows the simulated speciation of Fe(III) (100  $\mu\text{M}$ ) as a function of pH in the presence of Glu (10 -20  $\mu\text{M}$ ). The Fe(III)-aqua, Fe(III)-hydroxy complexes, and Fe(III)-Glu complexes were observed as a function of the pH. At pH = 3.8,  $[\text{Fe(III)}] = [\text{Glu}] = 100 \mu\text{M}$ , the Fe(III)-hydroxy complexes  $\text{Fe(OH)}^{2+}$  and  $\text{Fe(OH)}_2^+$  represent 24.4 and 22.8 % of the total Fe(III) concentration, respectively. In contrast, Fe(III)-Glu complex accounts for 52.3 % of the total Fe(III), while Fe(III)-aqua complex constitutes only 0.5 %. The UV-Vis spectra of Fe(III), Glu, and Fe(III)-Glu complex are depicted in **Fig. SM2**. The characteristic absorption band of Fe(III) with a maximum at 297 nm, corresponding to the charge transfer bands of  $\text{Fe(OH)}^{2+}$ , becomes attenuated in the presence of Glu. Moreover, the UV-Vis spectrum of Fe(III)-Glu mixture



differs from those of Fe(III) and Glu alone or the simple overlap of their individual spectra, confirming the formation of a stable Fe(III)-Glu complex (Samavat et al., 2007). The fractions of the generated complex in the presence of different Glu concentrations at pH = 3.8 are given in **Table SM5**. For the sake of simplicity, Fe(III)/Fe(II)-hydroxy and Fe(III)/Fe(II)-aqua complexes are hereafter referred as Fe(III) and Fe(II).

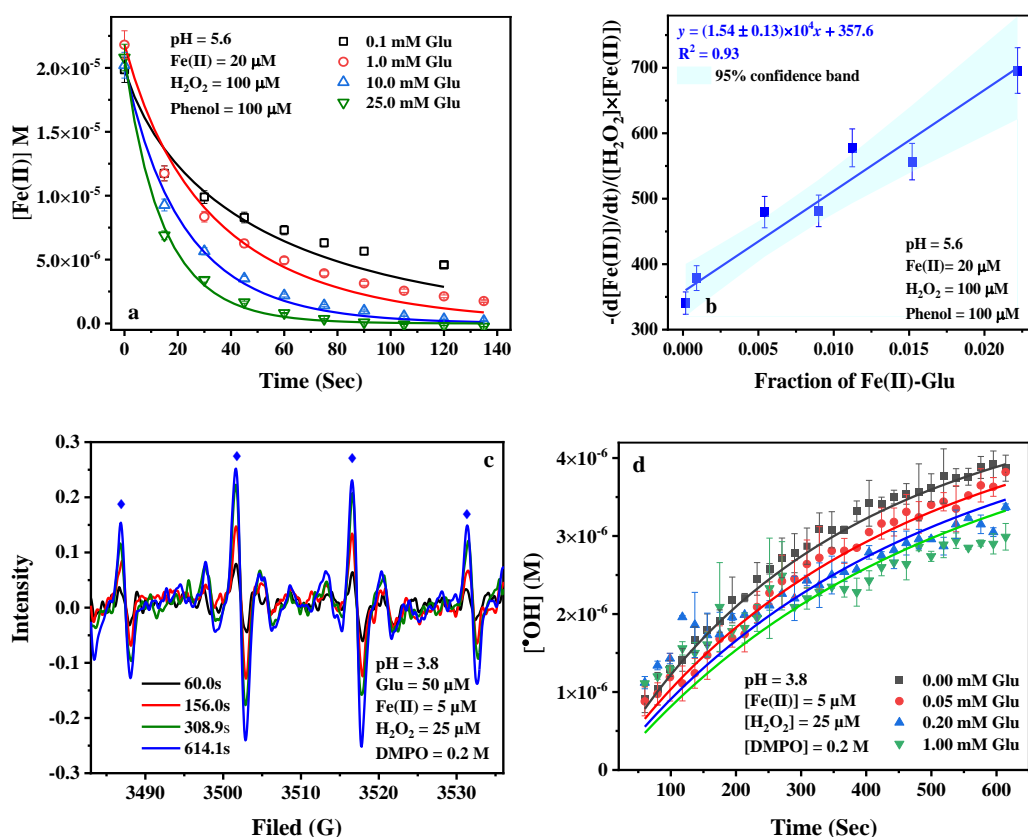
### 3.2. Fenton reaction process in the presence of Glu

#### 3.2.1. Fe(II) oxidation

To study the effect of Glu on the kinetics of the Fenton reaction and determine the rate constant of the reaction of Fe(II)-Glu with H<sub>2</sub>O<sub>2</sub>, experiments were performed using different concentrations of Glu. **Fig. 1a** shows the faster Fe(II) concentration decreases when the Glu concentration increases, which indicates that Glu can increase the reaction rate of Fe(II) with H<sub>2</sub>O<sub>2</sub>. This is likely due to the formation of the Fe(II)-Glu complex which has a high reaction rate constant with H<sub>2</sub>O<sub>2</sub>. As seen in **Fig. 1b**, the data obtained by plotting  $\frac{-\frac{d[\text{Fe(II)}]}{dt}}{[\text{H}_2\text{O}_2][\text{Fe(II)}]}$  as a function of the fraction of Fe(II)-Glu can be fitted with a linear equation  $y = ax + b$ , where  $a$  is equal to  $1.54 \pm 0.13 \times 10^4 \text{ M}^{-1} \text{ s}^{-1}$  and represents the rate constant of reaction of Fe(II)-Glu with H<sub>2</sub>O<sub>2</sub>, and  $b$  is equal to rate constant of Fe(II) with H<sub>2</sub>O<sub>2</sub> ( $-\frac{d[\text{Fe(II)}]}{dt}$  data is provided in **Table SM4**). This value is much higher than the rate constant of the classic Fenton reaction which has a rate constant of about  $50\text{-}70 \text{ M}^{-1} \text{ s}^{-1}$  (Kremer, 2003; Neyens and Baeyens, 2003; Rachmilovich-Calis et al., 2009). The reason behind this increase is likely due to the Fe(II)-Glu complex accessing a lower reduction potential calculated to be + 0.241 V compared with the Fe(II) (+0.771 V) (Strathmann and Stone, 2002), which contributes to the higher rate constant of the reaction of Fe(II)-Glu with H<sub>2</sub>O<sub>2</sub>.



265 Then the Fenton reaction model was used to fit the experimental data to verify the rate constant  
266 value of the reaction between Fe(II)-Glu and H<sub>2</sub>O<sub>2</sub>. As shown in **Fig. 1a**, the experimental data  
267 of Fe(II) kinetics can be well-fitted by the model. The fitted rate constant value of the reaction  
268 between Fe(II)-Glu and H<sub>2</sub>O<sub>2</sub> was obtained at a range of  $1.2 \times 10^4$  to  $1.8 \times 10^4$  M<sup>-1</sup> s<sup>-1</sup>, which is  
269 very close to the experimental results.



271 **Fig. 1** Effect of different concentrations of Glu on the kinetics of Fenton reaction (a), apparent  
272 rate constant as a function of the fraction of Fe(II)-Glu (b), Signal of EPR corresponding to  
273 DMPO-OH (The symbol "◆" marks the position of the characteristic 1:2:2:1 EPR signal of  
274 the DMPO-OH adduct.) (c), the kinetics of •OH generation in Fenton reaction in the presence  
275



276 *of different concentrations of Glu, (d). Points are determined experimentally, and lines in*  
277 *figures a and d are the fit of data using the kinetic model.*

### 278 3.2.2. •OH quantification

279 To study the effect of Glu on the •OH generation, EPR experiments were carried out. **Fig. 1c**  
280 shows the EPR signal of DMPO-OH (1:2:2:1) increases with the reaction time, indicating that  
281 •OH is continuously generated. In **Fig. 1d**, the concentration of generated •OH decreases when  
282 the Glu concentration increases from 0 to 1.0 mM. This trend suggests no direct •OH generation  
283 occurs from the reaction of Fe(II)-Glu with H<sub>2</sub>O<sub>2</sub>. This hypothesis has been verified by  
284 employing a kinetic model. The experimental data can be well fitted using the experimental rate  
285 constant  $k_{\text{Fe(II)-Glu/H}_2\text{O}_2} = 1.54 \pm 0.13 \times 10^4 \text{ M}^{-1} \text{ s}^{-1}$ .

## 286 3.3. Fe(III) photolysis in the presence of Glu

### 287 3.3.1. Fe(II) formation

288 To study the effect of Glu on the kinetics and determine the quantum yield of the photolysis of  
289 Fe(III), the photo-driven reaction was carried out in the presence of different concentrations of  
290 Glu (0-200 μM) under simulated solar light. **Fig. SM5a** shows that the Fe(II) generation rate  
291 decreases when the Glu concentration increases, which indicates that Glu slightly reduces the  
292 photoactivity of Fe(III). As shown in **Fig. 2a**, plotting the apparent quantum yield of Fe(II),  
293  $\Phi_{\text{Fe(II)}}^{\text{obs}}$ , as a function of the fraction of Fe(III)-Glu complex, the quantum yield of Fe(II)  
294 decreases with the fraction of Fe(III)-Glu complex increasing. The linear fit can depict the  
295 kinetic data well with a regression coefficient equal to 0.99. As mentioned in **SM2**, the intercept  
296 represents the Fe(II) quantum yield of Fe(III) photolysis under polychromatic irradiation, which



is equal to  $0.216 \pm 0.004$ . This result is consistent with previous data (Bossmann et al., 1998). The slope represents the difference between Fe(II) quantum yield of the Fe(III) photolysis and the value of the photolysis of Fe(III)-Glu complex ( $\Phi_{\text{Fe(III)-Glu}}^{\text{Fe(II)}} - \Phi_{\text{Fe(III)}}^{\text{Fe(II)}}$ ), which is equal to -0.179, hence the Fe(II) quantum yield during the photolysis of Fe(III)-Glu is calculated to be  $0.037 \pm 0.004$ . Weller et al. (Weller et al., 2013) investigated the photolysis of Fe(III)-carboxylate complexes and found the quantum yield of Fe(II) formation from Fe(III)-malonate at 308 nm and 351 nm, with values of  $0.024 \pm 0.001$  and  $0.040 \pm 0.003$  respectively. This suggests that Fe(III) complexes containing unsubstituted carboxylates as a functional group exhibit lower quantum yields compared to Fe(III).

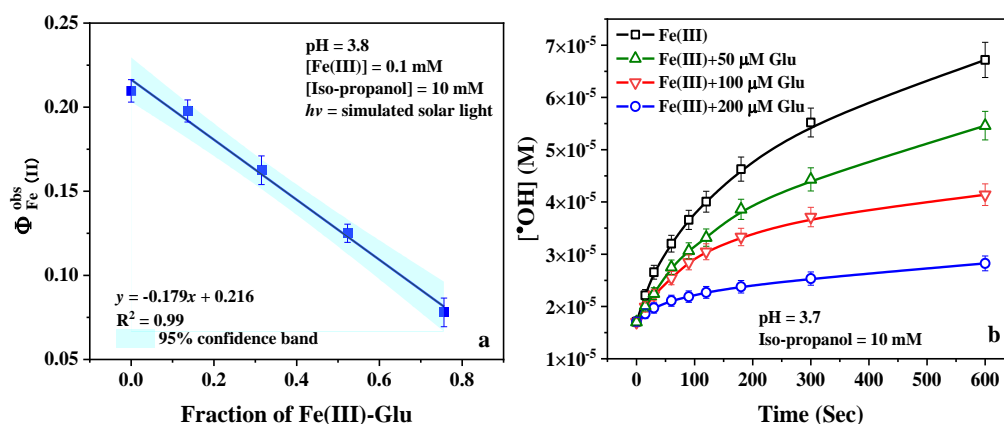


**Fig. 2** a) The quantum yield of Fe(III) photolysis as a function of the fraction of Fe(III)-Glu complex; b) The  $\cdot\text{OH}$  generation of Fe(III) photolysis in the presence of different concentrations of Glu. The continuous lines are visual guides generated by applying the "Connect B-Spline" function in Origin 2019.

### 3.3.2. $\cdot\text{OH}$ generation



312 Since the photolysis of Fe(III) is an important process affecting the budget of  $\bullet\text{OH}$  in the  
313 atmosphere (Guo et al., 2014), the effect of Glu on the  $\bullet\text{OH}$  produced by the photolysis process  
314 of Fe(III) was investigated. As shown in **Fig. SM5b**, the acetone generation rate decreases when  
315 the Glu concentration increases, indicating that the  $\bullet\text{OH}$  generation of the Fe(III) photolysis  
316 decreases in the presence of Glu (**Fig. 2b**). The most likely reason for this observation is the  
317 decrease of the Fe(III) hydroxy complexes (**Table SM5**), hence the decrease of the  $\bullet\text{OH}$  yield  
318 as the Fe(III)-Glu does not produce  $\bullet\text{OH}$  directly, but instead forms Glu oxidation products  
319 ( $\text{Glu}_{\text{ox}}$ ) through the LMCT process. These Glu oxidation products can complex Fe(II) and  
320 regenerate Fe(III), a mechanism known as “the quenching mechanism” proposed by Wang et  
321 al (2010)(Wang et al., 2010). This process reduces the apparent quantum yield of Fe(II) to  $0.037$   
322  $\pm 0.004$ . This result illustrates that  $\bullet\text{OH}$  generation could be less in the presence of amino acids  
323 during the daytime in the atmosphere.

#### 324 **3.4. The Glu fate in the presence of Fe(III) under simulated solar light**

##### 325 **3.4.1 Photodegradation of Glutamic acid in different systems**

326 All the above results indicate that Glu not only stabilizes Fe(III)/Fe(II) at higher pH but also  
327 influences the Fenton reaction and photolysis of Fe(III) processes. The main effects were that  
328 the complexes altered the individual reaction rate constants and  $\bullet\text{OH}$  production.

329 On the other hand, Glu as the organic ligand can also be degraded during the reaction, especially  
330 photo-reaction in the atmosphere. **Fig. 3** shows the photodegradation kinetics of Glu in different  
331 systems, and the first-order fitted data is reported in **Fig. SM6**. As expected, when only Glu  
332 was present in the solution, no significant degradation was observed after 1 hour of irradiation,  
333 as shown by the UV-Vis spectrum (**Fig. SM2**) of Glu, as there is no significant absorption of





solar radiation. The Glu degradation efficiency slightly increased in the presence of 1 mM H<sub>2</sub>O<sub>2</sub> with a degradation constant of  $2.44 \pm 0.45 \times 10^{-5} \text{ s}^{-1}$  corresponding with a degradation of 8.5 % in 1 hour, which is due to the formation of  $\bullet\text{OH}$  radicals via the photolysis of H<sub>2</sub>O<sub>2</sub>. In addition, the rate constant of  $\bullet\text{OH}$  with Glu is  $2.3 \times 10^8 \text{ M}^{-1} \text{ s}^{-1}$  (Masuda et al., 1973), which means that the reaction between those two components is one of the most important processes for the degradation of Glu. Considering the second reaction rate constant between  $\bullet\text{OH}$  and H<sub>2</sub>O<sub>2</sub> ( $k_{\text{H}_2\text{O}_2}^{\bullet\text{OH}} = 2.7 \times 10^7 \text{ M}^{-1} \text{ s}^{-1}$ ) (Christensen et al., 1982), it can be argued that under adopted conditions, about 55 % of generated  $\bullet\text{OH}$  was quenched by the H<sub>2</sub>O<sub>2</sub>, which led to the formation of less reactive hydroperoxyl radical/superoxide anion pair (HO<sub>2</sub> $\bullet$ /O<sub>2</sub> $\bullet^-$ ).

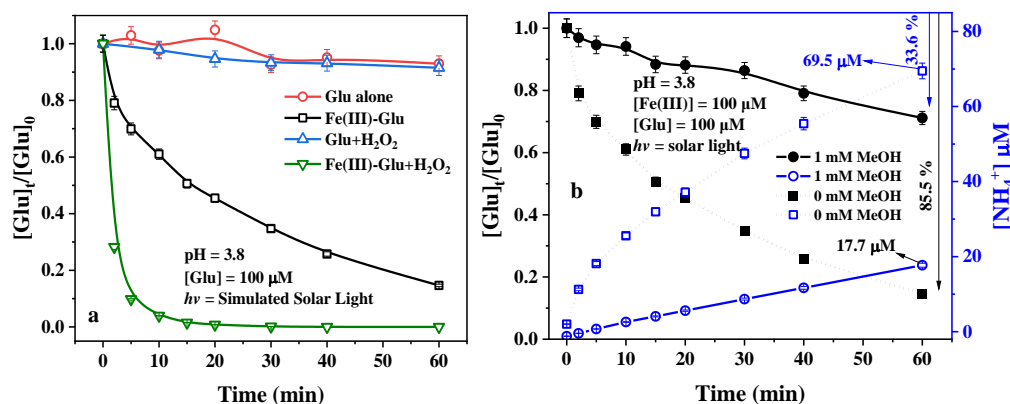


**Fig. 3** Photodegradation of Glu in different systems: Fe(III)-Glu; Glu+H<sub>2</sub>O<sub>2</sub> and Fe(III)-Glu+H<sub>2</sub>O<sub>2</sub> ([Glu] = 100 μM, [Fe(III)] = 100 μM, [H<sub>2</sub>O<sub>2</sub>] = 1 mM). The continuous lines are visual guides generated by applying the "Connect B-Spline" function in Origin 2019.

Moreover, in the presence of Fe(III), the mixture of Fe(III)-hydroxy and Fe(III)-Glu complexes underwent the photolysis process. As shown in **Fig. 3a**, about 85 % of Glu was degraded with a first-order rate constant of  $4.99 \pm 0.24 \times 10^{-4} \text{ s}^{-1}$  after 1 hour of irradiation. This high efficiency



350 is likely due to two different Glu degradation pathways, one is due to the reaction between Glu  
351 and the  $\bullet\text{OH}$  radicals generated by photolysis of Fe(III) (R1 and R2), and the other one is due  
352 to the direct photolysis of Fe(III)-Glu leading to the formation of Fe(II) and oxidation products  
353 of the organic ligand ( $\text{Glu}_{\text{ox}}$ ). The synergistic effect of those two processes highly improved the  
354 Glu degradation efficiency. To distinguish between the contributions of the two degradation  
355 pathways, methanol was selected as  $\bullet\text{OH}$  scavenger ( $k_{\bullet\text{OH}}^{\text{Methanol}} = 9.7 \times 10^8 \text{ M}^{-1} \text{ s}^{-1}$ ) (Buxton et al.,  
356 1988). As illustrated in **Fig. 3b**, Glu degradation was inhibited by 60 %, indicating that 40 %  
357 of Glu degradation originates from the photolysis of Fe(III)-Glu complexes. Interestingly, this  
358 ratio aligns with the proportion of Fe(III) and Fe(III)-Glu complexes in the system (**Table SM5**),  
359 confirming the aforementioned conclusion. Furthermore, the degradation of Glu resulting from  
360 the photolysis of Fe(III)-Glu complexes likely does not involve a  $\bullet\text{OH}$  process (Sun et al., 1998;  
361 Weller et al., 2013).

362 Glu degradation was observed to be approximately 100 % after 20 mins of irradiation in the  
363 presence of Fe(III) and  $\text{H}_2\text{O}_2$ , with a first-order rate constant of  $5.13 \pm 1.03 \times 10^{-3} \text{ s}^{-1}$ . Compared  
364 to conditions with only Fe(III) or  $\text{H}_2\text{O}_2$ , the efficiency of Glu degradation significantly improves  
365 due to the photo-Fenton reaction in the system, which greatly accelerates the formation rate of  
366 reactive species and consequently enhances the degradation rate of Glu.

### 367 **3.4.2. Analysis of photodegradation products of glutamic acid**

368 To distinguish the Glu degradation processes resulting from the photolysis of Fe(III)-Glu  
369 complexes and from those caused by  $\bullet\text{OH}$  attack, which might lead to the formation of different  
370 products, a series of experiments were conducted. In all cases, IC-MS was employed to analyze  
371 the formation of short-chain carboxylic acid and ammonium ions, providing a deeper



372 understanding of the photochemical reaction products in various systems under simulated solar  
373 light.

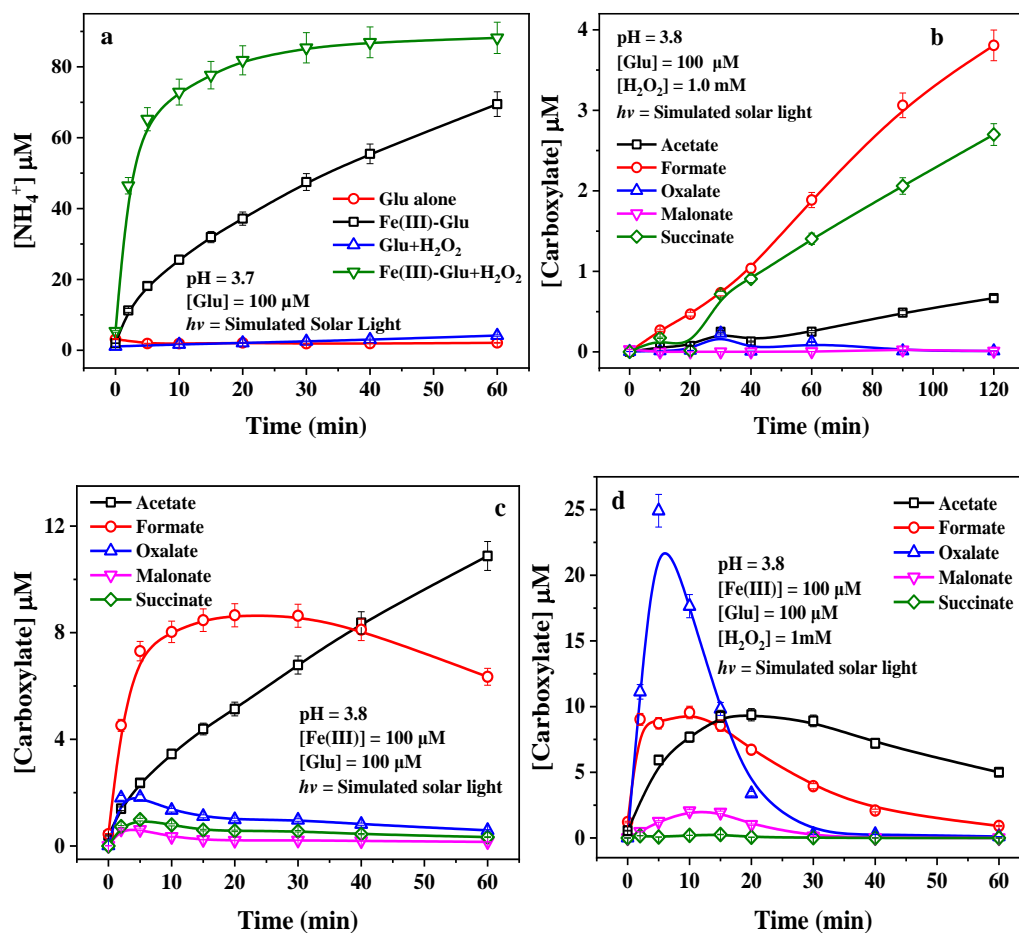
374 **Figure 4a** depicts the formation of ammonium ( $\text{NH}_4^+$ ) in different systems under irradiation. A  
375 positive correlation is observed between the rate of  $\text{NH}_4^+$  production and the rate of Glu  
376 degradation in various systems, suggesting the occurrence of deamination during the Glu  
377 degradation. Additionally, several carboxylic acids (i.e. acetic, formic, succinic, malonic, and  
378 oxalic acids) were detected (**Table SM6**), as illustrated in **Fig. 4b**, **4c**, and **4d**. Notably, the  
379 concentration of generated carboxyl acids is considerably lower than that of  $\text{NH}_4^+$ .

380 After 120 min of irradiation, low concentrations of generated  $\text{NH}_4^+$  and carboxylic acid were  
381 determined during Glu photolysis due to small Glu degradation (see **Fig. 4a** and **Fig. SM7**). In  
382 the presence of 1 mM  $\text{H}_2\text{O}_2$ ,  $\text{NH}_4^+$  concentration increased to 7.8  $\mu\text{M}$  within 120 min,  
383 representing a 3-fold increase compared to that produced during Glu photolysis. **Fig. 4b**  
384 demonstrates the formation of carboxylic acids with formate and succinate as primary  
385 carboxylate products, while a negligible concentration of acetate (less than 1  $\mu\text{M}$ ) was also  
386 detected, all of which are products of  $\bullet\text{OH}$  attack.

387 In the presence of Fe(III),  $\text{NH}_4^+$  concentration increased to 69.5  $\mu\text{M}$  (**Fig. 4a**) within 60 min.  
388 Simultaneously, the generation of carboxyl acids, such as formate, acetate, and oxalate was  
389 observed. The concentration of formate initially increased, reaching a plateau value of 8.7  $\mu\text{M}$   
390 at 20 min, after decreasing to approximately 6.4  $\mu\text{M}$  at 60 min. The reason for the decline is  
391 probably the reaction to photo-generated  $\bullet\text{OH}$ . Acetate concentration increased throughout the  
392 reaction, reaching 10.9  $\mu\text{M}$  at 60 min. Other carboxylates, such as succinate, malonate, and  
393 oxalate, were found in lower concentration, with a maximum of around 2  $\mu\text{M}$  within 5 min. As  
394 mentioned above, in the presence of Fe(III), the Glu degradation can be attributed to two



395 pathways: one resulting from  $\bullet\text{OH}$  attack, on the other from the photolysis of the Fe(III)-Glu  
396 complexes.



398  
399 **Fig. 4.** The by-products of Glu degradation under solar light a) formation of  $\text{NH}_4^+$  in different  
400 systems; formation of carboxylic acids b) in the system Glu +  $\text{H}_2\text{O}_2$ ; c) in the system Glu +  
401 Fe(III) and d) in the system Glu + Fe(III) +  $\text{H}_2\text{O}_2$ . The continuous lines are visual guides  
402 generated by applying the "Connect B-Spline" function in Origin 2019.

403 To distinguish the contribution of these two pathways, isopropanol was employed to quench  
404  $\bullet\text{OH}$  in solution generating acetone as the main product (Motohashi and Saito, 1993). As shown



in **Fig. SM8**, only acetate and formate were generated (succinate, malonate, and oxalate were not detected). Moreover, the presence of isopropanol significantly enhanced the formation of acetate compared to values observed with only Fe(III) and Glu. This is likely due to the H-donor effect of the added alcohol or to the reaction between acetic acid radicals ( $\text{HOOCCH}_2^\bullet$ ) and  $\text{HO}_2^\bullet$  radicals, the latter being generated through the reaction of  $^\bullet\text{OH}$  with the alcohol. As shown in **Fig. SM8**, the concentration of generated formate in the presence of isopropanol and Fe(III) is lower than that when only Fe(III) is added, suggesting that formate was likely not a primary product generated from the photolysis of Fe(III)-Glu complexes but rather may be produced by  $^\bullet\text{OH}$  attack of other carboxylic acids. For example, the generated acetate can be further oxidized reacting with  $^\bullet\text{OH}$  leading to the formation of formate.

This finding is consistent with the result observed in the presence of  $\text{H}_2\text{O}_2$  alone (**Fig. SM7**). In the presence of  $^\bullet\text{OH}$  scavenger, the generation of  $\text{NH}_4^+$  was strongly inhibited with the formation of  $17.7\ \mu\text{M}$  instead of  $69.5\ \mu\text{M}$  after 1 h (as previously reported in **Fig. 3b**), which indicates that the  $\text{NH}_4^+$  formation is mainly due to the  $^\bullet\text{OH}$  attack process. Furthermore, a significant  $\text{NH}_4^+$  (up to  $69.5\ \mu\text{M}$  within 60 min) can be observed in the presence of both Fe(III) and  $\text{H}_2\text{O}_2$  (**Fig. 4d**). Oxalate, acetate, and formate were observed as the predominant carboxylate products with higher concentrations, reaching  $24.9$ ,  $9.4$ , and  $9.6\ \mu\text{M}$  respectively, before decreasing. Additionally, the formations of malonate ( $2.1\ \mu\text{M}$ ) and succinate ( $0.3\ \mu\text{M}$ ) were observed at lower concentrations during the photoreaction. In the presence of  $\text{H}_2\text{O}_2$  and Fe(III), the Fe(III)/Fe(II)-cycle is enhanced via the photo-Fenton reaction. Fe(II) is rapidly re-oxidized to Fe(III) to produce  $^\bullet\text{OH}$ , which then directly attacks Glu, leading to degradation. Fe(III) is re-complexed by Glu reactivating the photoreaction and then the iron cycle. Therefore, the addition of  $\text{H}_2\text{O}_2$  favors deamination as well as various carbon-centered radical combination



interactions. The rapid depletion of oxalate after 30 min implies that photolysis of complexes between Fe(III) and polycarboxylic acid also occurs in this system, while formate, acetate, and malonate exhibit similar tendencies with different reaction rates. To verify the mineralization of Glu during the reaction, a TOC was followed during the reaction. As shown in **Fig. SM9a**, the mineralization efficiency of Glu in the presence of Fe(III) and H<sub>2</sub>O<sub>2</sub> is significantly higher than that observed when only Fe(III) is present, due to the presence of the photo-Fenton process. This finding is consistent with the degradation efficiency of Glu presented in **Figure 3a**. Hence, these results illustrate that Glu was mineralized to form CO<sub>2</sub> and H<sub>2</sub>O. Moreover, the TOC values obtained experimentally are higher than the values calculated from the concentration of Glu and carboxylic acid products, indicating the presence of other organic compounds in the system. Along these organic substances cannot be detected under our experimental conditions, they will enter the cloud water gas phase, further participating in atmospheric photochemical reactions and eventually being mineralized into H<sub>2</sub>O and CO<sub>2</sub>. In the presence of H<sub>2</sub>O<sub>2</sub>, as Glu undergoes photodegradation, the concentration of H<sub>2</sub>O<sub>2</sub> in the system continues to decrease until it is completely consumed (**Fig. SM9b**).

### 3.5. Insight into the mechanism of Glu transformation

The light-driven transformation mechanism of Glu in the presence of Fe(III) was investigated, with a focus on the <sup>•</sup>OH-mediated and the ligand-to-metal charge transfer (LMCT) process. The key difference between the two processes lies in the generation of glutamate radicals: the <sup>•</sup>OH-mediated process involves a free radical mechanism initiated by hydrogen abstraction, whereas the LMCT pathway proceeds via an electron transfer process driven by photoexcitation. To provide a clear comparison, the two mechanisms are illustrated separately in **Scheme. 1**

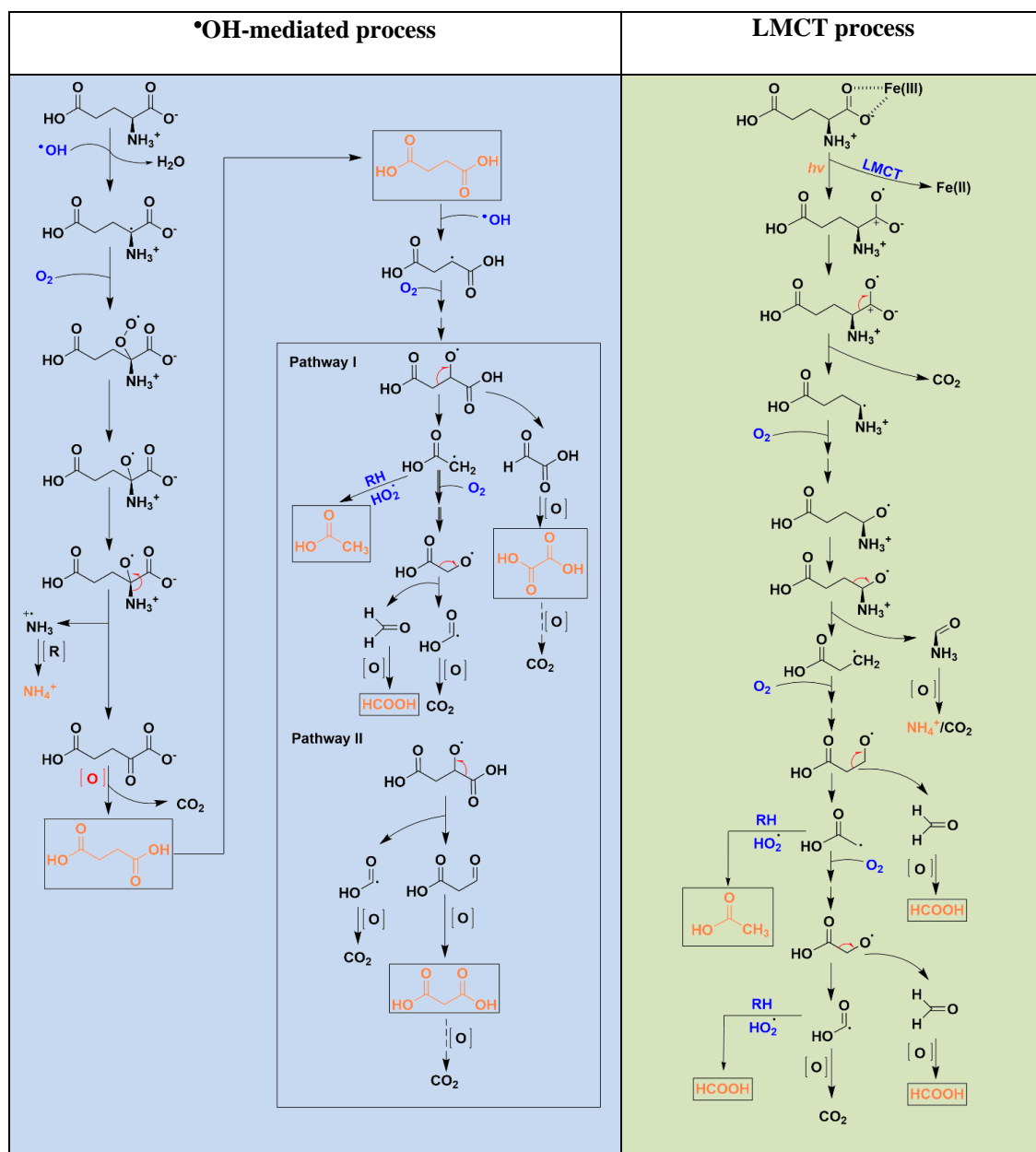


450 summarizing the possible Glu degradation pathway, derived from IC-MS analysis of the  
451 detected products.

452 In the  $\bullet\text{OH}$ -mediated process, the  $\alpha$ - carbon of Glu is identified as the primary site attacked for  
453  $\bullet\text{OH}$  attack, initiating the transformation process. Hydrogen abstraction by  $\bullet\text{OH}$  results in the  
454 formation of glutamate alkyl radical ( $\text{R-C}^\bullet(\text{COO}^-)\text{NH}_3^+$ ) and  $\text{H}_2\text{O}$ . Subsequently, this alkyl  
455 radical reacts with  $\text{O}_2$  to generate the alkylperoxy radical ( $\text{ROO}^\bullet$ ), which is further converted to  
456 alkoxy radical ( $\text{RO}^\bullet$ ) (Goldman et al., 2021; von Sonntag and Schuchmann, 1991). The  
457 formation of  $\text{RO}^\bullet$  is followed by a deamination process, which leads to the formation of  
458 ammonium ( $\text{NH}_4^+$ ) and 2-oxoadipic acid through the cleavage of the amino group. Due to the  
459 presence of an oxo group ( $\text{C}=\text{O}$ ) adjacent to a carboxyl group ( $\text{COOH}$ ), 2-oxoadipic acid is  
460 chemically unstable and prone to self-decomposition via decarboxylation, resulting in the  
461 formation of succinic acid (Penteado et al., 2019). Further oxidation of succinic acid produces  
462 smaller carboxylic acids.

463 In contrast, the LMCT process is initiated upon irradiation, resulting in the reduction of  $\text{Fe(III)}$   
464 to  $\text{Fe(II)}$  and the generation of a radical centered on the oxygen atom of  $\alpha$ -carboxyl group of  
465 glutamic acid ( $\text{R-CH}(\text{NH}_3^+)\text{C}^+\text{O}^\bullet\text{O}^-$ ). This high reactive radical undergoes a decarboxylation  
466 process resulting in the formation of an alkyl radical ( $\text{R-CH}^\bullet\text{NH}_3^+$ ). Subsequently, the radical  
467 chain reaction propagates in the presence of  $\text{O}_2$ , leading to the formation of smaller carboxylic  
468 acids. It is critical to highlight that the only carboxylic acids detected under the same conditions  
469 are formic acid and acetic acid. This is different from the  $\bullet\text{OH}$ -mediated process, in which  
470 succinate is first formed and then further decomposed into compounds such as other small  
471 molecular carboxylic acids.

472



**Scheme 1.** The mechanism of Glu degradation in the presence of Fe(III): by •OH attacking process and LMCT process. Products in orange are detected by IC-MS.





#### 476 4. ATMOSPHERIC IMPLICATION

477 This study systematically investigated the complexation of Glu with Fe(II)/Fe(III), its effect on  
478 the typical atmospheric reactions (Fenton reaction and Fe(III) photolysis), and its fate in the  
479 atmospheric aqueous phase. Our findings reveal that iron-amino acid complexes (Fe-AAs)  
480 significantly modify the Fe(II)/Fe(III) cycle and •OH budget, diverging from the "classic"  
481 photo-Fenton mechanisms. Specifically, Fe(II)-Glu reacts with H<sub>2</sub>O<sub>2</sub> at a rate constant two  
482 orders of magnitude higher than Fe(II) alone, potentially improving the iron cycle. Conversely,  
483 Fe(III)-Glu exhibits a lower quantum yield under irradiation, suppressing the Fe(III)/Fe(II)  
484 cycle. Moreover, both reactions result in lower •OH generation, as they favor the formation of  
485 Glu oxidation products (Glu<sub>ox</sub>) over •OH, thus partially affecting atmospheric oxidative  
486 capacity.

487 To date, the concentration of the Fe(II)/Fe(III)-Glu in cloud water has not yet been directly  
488 measured, hence, based on the reported mean concentrations of Glu (87 nM) (Renard et al.,  
489 2022), Fe(II) (1 µM) (Deguillaume et al., 2014), and Fe(III) (0.5 µM) (Deguillaume et al., 2014)  
490 in cloud water from the Puy de Dôme station (PUY - France), the fraction of Fe(II)-Glu and  
491 Fe(III)-Glu was calculated to be around  $8.7 \times 10^{-10}$  -  $2.1 \times 10^{-4}$  % and  $6.1 \times 10^{-2}$  -  $2.4 \times 10^{-1}$  % using  
492 Hyss software at pH = 3 - 7, respectively. Although the fraction of iron-Glu is likely low in  
493 cloud water conditions, the concentration of Glu in cloud droplets may increase during the cloud  
494 water evaporation, leading to an increase in the proportion of iron-Glu complexes. This shift  
495 could alter atmospheric Fenton reaction dynamics, reducing •OH production, particularly at  
496 night (Galloway et al., 2014; Shulman et al., 1997). Similarly, the lower quantum yield of the  
497 Fe(III)-Glu under irradiation inhibits the Fe(II)/Fe(III) cycle and •OH generation especially in  
498 daytime conditions. In addition, recent studies reported that the average AAs contribution



499 corresponded to 9.1 % of the dissolved organic carbon (DOC) (Bianco et al., 2016), highlighting  
500 their significance. Hence, Fe-AAs play a crucial role in iron speciation, stability, and  $\bullet\text{OH}$   
501 budget in atmospheric aqueous phases, which suggests that the inclusion of iron- Fe-AAs in  
502 atmospheric aqueous phase models is essential for a more precise estimation of  $\bullet\text{OH}$  production,  
503 which is central to understanding oxidation processes and secondary aerosol formation.

504 In addition, irradiation of Glu in the presence of Fe(III), demonstrated two different  
505 mechanisms ( $\bullet\text{OH}$  mediated and LMCT process) leading to the generation of different products,  
506 which can further influence the atmospheric chemical composition. Overall, the generation of  
507  $\text{NH}_4^+$  is regarded as a link between organic nitrogen species and inorganic nitrogen in cloud  
508 water. The generation of carboxylic acids further increases atmospheric complexity, as the  
509 generated carboxylic acids (e.g., oxalic acid) can be complex with iron and participate in the  
510 consequent photoreactions. In fact, atmospheric models often simplify the distribution and  
511 interactions of transition metal ions (TMIs) with organic compounds, including AAs. This study  
512 highlights the crucial role of the LMCT process in AAs oxidation, which could be considered  
513 in atmospheric modeling.

#### 514 **ACKNOWLEDGMENT**

515 This work was supported by the Agence Nationale de la Recherche of France in the frame of  
516 the PRCI project REACTE.

#### 517 **AUTHOR CONTRIBUTION**

518 **Peng Cheng:** Investigation, Formal analysis, Writing – original draft; **Gilles Mailhot:** Funding  
519 acquisition, Review & editing, Supervision; **Mohamed Sarakha:** Review & editing,  
520 Supervision, **Guillaume Voyard:** Technical support; **Daniele Scheres Firak:** Review &  
521 editing; **Thomas Schaefer:** Funding acquisition, review & editing; **Hartmut Herrmann:**



522 Review & editing; **Marcello Brigante**: Conceptualization, Writing-review & editing,  
523 Supervision.

## 524 REFERENCE

- 525 Alpert, P. A., Dou, J., Corral Arroyo, P., Schneider, F., Xto, J., Luo, B., Peter, T., Huthwelker,  
526 T., Borca, C. N., Henzler, K. D., Schaefer, T., Herrmann, H., Raabe, J., Watts, B., Krieger, U.  
527 K., and Ammann, M.: Photolytic radical persistence due to anoxia in viscous aerosol particles,  
528 Nature Communications, 12, 1769, <https://doi.org/10.1038/s41467-021-21913-x>, 2021.
- 529 Angle, K. J., Neal, E. E., and Grassian, V. H.: Enhanced Rates of Transition-Metal-Ion-  
530 Catalyzed Oxidation of S(IV) in Aqueous Aerosols: Insights into Sulfate Aerosol Formation in  
531 the Atmosphere, Environmental Science & Technology, 55, 10291–10299,  
532 <https://doi.org/10.1021/acs.est.1c01932>, 2021.
- 533 Bader, H., Sturzenegger, V., and Hoigné, J.: Photometric method for the determination of low  
534 concentrations of hydrogen peroxide by the peroxidase catalyzed oxidation of N,N-diethyl-*p*-  
535 phenylenediamine (DPD), Water Research, 22, 1109–1115, [https://doi.org/10.1016/0043-](https://doi.org/10.1016/0043-1354(88)90005-X)  
536 1354(88)90005-X, 1988.
- 537 Battaglia Jr., M. A., Weber, R. J., Nenes, A., and Hennigan, C. J.: Effects of water-soluble  
538 organic carbon on aerosol pH, Atmospheric Chemistry and Physics, 19, 14607–14620,  
539 <https://doi.org/10.5194/acp-19-14607-2019>, 2019.
- 540 Bianco, A., Passananti, M., Perroux, H., Vyard, G., Mouchel-Vallon, C., Chaumerliac, N.,  
541 Mailhot, G., Deguillaume, L., and Brigante, M.: A better understanding of hydroxyl radical  
542 photochemical sources in cloud waters collected at the puy de Dôme station – experimental  
543 versus modelled formation rates, Atmospheric Chemistry and Physics, 15, 9191–9202,  
544 <https://doi.org/10.5194/acp-15-9191-2015>, 2015.
- 545 Bianco, A., Vyard, G., Deguillaume, L., Mailhot, G., and Brigante, M.: Improving the  
546 characterization of dissolved organic carbon in cloud water: Amino acids and their impact on  
547 the oxidant capacity, Scientific Reports, 6, 37420, <https://doi.org/10.1038/srep37420>, 2016.
- 548 Bianco, A., Vaïtilingom, M., Bridoux, M., Chaumerliac, N., Pichon, J.-M., Piro, J.-L., and  
549 Deguillaume, L.: Trace Metals in Cloud Water Sampled at the Puy De Dôme Station,  
550 Atmosphere, 8, 225, <https://doi.org/10.3390/atmos8110225>, 2017.
- 551 Bianco, A., Deguillaume, L., Vaïtilingom, M., Nicol, E., Baray, J.-L., Chaumerliac, N., and  
552 Bridoux, M.: Molecular Characterization of Cloud Water Samples Collected at the Puy de  
553 Dôme (France) by Fourier Transform Ion Cyclotron Resonance Mass Spectrometry,  
554 Environmental Science & Technology, 52, 10275–10285,  
555 <https://doi.org/10.1021/acs.est.8b01964>, 2018.
- 556 Bianco, A., Passananti, M., Brigante, M., and Mailhot, G.: Photochemistry of the Cloud  
557 Aqueous Phase: A Review, Molecules, 25, 423, <https://doi.org/10.3390/molecules25020423>,  
558 2020.



- 559 Bossmann, S. H., Oliveros, E., Göb, S., Siegwart, S., Dahlen, E. P., Payawan, L., Straub, M.,  
560 Wörner, M., and Braun, A. M.: New Evidence against Hydroxyl Radicals as Reactive  
561 Intermediates in the Thermal and Photochemically Enhanced Fenton Reactions, *The Journal of*  
562 *Physical Chemistry A*, 102, 5542–5550, <https://doi.org/10.1021/jp980129j>, 1998.
- 563 Buxton, G. V., Greenstock, C. L., Helman, W. P., and Ross, A. B.: Critical Review of rate  
564 constants for reactions of hydrated electrons, hydrogen atoms and hydroxyl radicals ( $\cdot\text{OH}/\cdot\text{O}-$   
565 in Aqueous Solution, *Journal of Physical and Chemical Reference Data*, 17, 513–886,  
566 <https://doi.org/10.1063/1.555805>, 1988.
- 567 Christensen, H., Sehested, K., and Corfitzen, H.: Reactions of hydroxyl radicals with hydrogen  
568 peroxide at ambient and elevated temperatures, *The Journal of Physical Chemistry*, 86, 1588–  
569 1590, <https://doi.org/10.1021/j100206a023>, 1982.
- 570 Deguillaume, L., Charbouillot, T., Joly, M., Vaïtilingom, M., Parazols, M., Marinoni, A.,  
571 Amato, P., Delort, A.-M., Vinatier, V., Flossmann, A., Chaumerliac, N., Pichon, J. M., Houdier,  
572 S., Laj, P., Sellegri, K., Colomb, A., Brigante, M., and Mailhot, G.: Classification of clouds  
573 sampled at the puy de Dôme (France) based on 10 yr of monitoring of their physicochemical  
574 properties, *Atmospheric Chemistry and Physics*, 14, 1485–1506, [https://doi.org/10.5194/acp-](https://doi.org/10.5194/acp-14-1485-2014)  
575 14-1485-2014, 2014.
- 576 Edwards, K. C., Klodt, A. L., Galeazzo, T., Schervish, M., Wei, J., Fang, T., Donahue, N. M.,  
577 Aumont, B., Nizkorodov, S. A., and Shiraiwa, M.: Effects of Nitrogen Oxides on the Production  
578 of Reactive Oxygen Species and Environmentally Persistent Free Radicals from  $\alpha$ -Pinene and  
579 Naphthalene Secondary Organic Aerosols, *The Journal of Physical Chemistry A*, 126, 7361–  
580 7372, <https://doi.org/10.1021/acs.jpca.2c05532>, 2022.
- 581 Gabet, A., Guy, C., Fazli, A., Métivier, H., de Brauer, C., Brigante, M., and Mailhot, G.: The  
582 ability of recycled magnetite nanoparticles to degrade carbamazepine in water through photo-  
583 Fenton oxidation at neutral pH, *Separation and Purification Technology*, 317, 123877,  
584 <https://doi.org/10.1016/j.seppur.2023.123877>, 2023.
- 585 Galloway, M. M., Powelson, M. H., Sedehi, N., Wood, S. E., Millage, K. D., Kononenko, J. A.,  
586 Rynaski, A. D., and De Haan, D. O.: Secondary Organic Aerosol Formation during Evaporation  
587 of Droplets Containing Atmospheric Aldehydes, Amines, and Ammonium Sulfate,  
588 *Environmental Science & Technology*, 48, 14417–14425, <https://doi.org/10.1021/es5044479>,  
589 2014.
- 590 Gligorovski, S., Strekowski, R., Barbati, S., and Vione, D.: Environmental Implications of  
591 Hydroxyl Radicals ( $(\cdot)\text{OH}$ ), *Chemical Reviews*, 115, 13051–13092,  
592 <https://doi.org/10.1021/cr500310b>, 2015.
- 593 Goldman, M. J., Green, W. H., and Kroll, J. H.: Chemistry of Simple Organic Peroxy Radicals  
594 under Atmospheric through Combustion Conditions: Role of Temperature, Pressure, and  $\text{NO}_x$   
595 Level, *The Journal of Physical Chemistry A*, 125, 10303–10314,  
596 <https://doi.org/10.1021/acs.jpca.1c07203>, 2021.
- 597 Guo, J., Tilgner, A., Yeung, C., Wang, Z., Louie, P. K. K., Luk, C. W. Y., Xu, Z., Yuan, C.,  
598 Gao, Y., Poon, S., Herrmann, H., Lee, S., Lam, K. S., and Wang, T.: Atmospheric Peroxides in  
599 a Polluted Subtropical Environment: Seasonal Variation, Sources and Sinks, and Importance of



- 600 Heterogeneous Processes, *Environmental Science & Technology*, 48, 1443–1450,  
601 <https://doi.org/10.1021/es403229x>, 2014.
- 602 Hoops, S., Sahle, S., Gauges, R., Lee, C., Pahle, J., Simus, N., Singhal, M., Xu, L., Mendes, P.,  
603 and Kummer, U.: COPASI—a COMplex PATHway SIMulator, *Bioinformatics*, 22, 3067–3074,  
604 <https://doi.org/10.1093/bioinformatics/btl485>, 2006.
- 605 Kanakidou, M., Myriokefalitakis, S., and Tsigaridis, K.: Aerosols in atmospheric chemistry and  
606 biogeochemical cycles of nutrients, *Environmental Research Letters*, 13, 063004,  
607 <https://doi.org/10.1088/1748-9326/aabddb>, 2018.
- 608 Kremer, M. L.: The Fenton Reaction. Dependence of the Rate on pH, *The Journal of Physical*  
609 *Chemistry A*, 107, 1734–1741, <https://doi.org/10.1021/jp020654p>, 2003.
- 610 Long, Y., Charbouillot, T., Brigante, M., Mailhot, G., Delort, A.-M., Chaumerliac, N., and  
611 Deguillaume, L.: Evaluation of modeled cloud chemistry mechanism against laboratory  
612 irradiation experiments: The  $\text{H}_2\text{O}_2$ /iron/carboxylic acid chemical system, *Atmospheric*  
613 *Environment*, 77, 686–695, <https://doi.org/10.1016/j.atmosenv.2013.05.037>, 2013.
- 614 Mace, K. A., Kubilay, N., and Duce, R. A.: Organic nitrogen in rain and aerosol in the eastern  
615 Mediterranean atmosphere: An association with atmospheric dust, *Journal of Geophysical*  
616 *Research: Atmospheres*, 108, <https://doi.org/10.1029/2002JD002997>, 2003.
- 617 Marion, A., Brigante, M., and Mailhot, G.: A new source of ammonia and carboxylic acids in  
618 cloud water: The first evidence of photochemical process involving an iron-amino acid complex,  
619 *Atmospheric Environment*, 195, 179–186, <https://doi.org/10.1016/j.atmosenv.2018.09.060>,  
620 2018.
- 621 Masuda, T., Nakano, S., and Kondo, M.: Rate constants for the reactions of OH radicals with  
622 the enzyme proteins as determined by the p-nitrosodimethylaniline method, *Journal of*  
623 *Radiation Research*, 14, 339–345, <https://doi.org/10.1269/jrr.14.339>, 1973.
- 624 Matos, J. T. V., Duarte, R. M. B. O., and Duarte, A. C.: Challenges in the identification and  
625 characterization of free amino acids and proteinaceous compounds in atmospheric aerosols: A  
626 critical review, *TrAC Trends in Analytical Chemistry*, 75, 97–107,  
627 <https://doi.org/10.1016/j.trac.2015.08.004>, 2016.
- 628 Motohashi, N. and Saito, Y.: Competitive Measurement of Rate Constants for Hydroxyl Radical  
629 Reactions Using Radiolytic Hydroxylation of Benzoate, *Chemical & Pharmaceutical Bulletin*,  
630 41, 1842–1845, <https://doi.org/10.1248/cpb.41.1842>, 1993.
- 631 Neyens, E. and Baeyens, J.: A review of classic Fenton’s peroxidation as an advanced oxidation  
632 technique, *Journal of Hazardous Materials*, 98, 33–50, [https://doi.org/10.1016/S0304-](https://doi.org/10.1016/S0304-3894(02)00282-0)  
633 [3894\(02\)00282-0](https://doi.org/10.1016/S0304-3894(02)00282-0), 2003.
- 634 Penteado, F., Lopes, E. F., Alves, D., Perin, G., Jacob, R. G., and Lenardão, E. J.:  $\alpha$ -Keto Acids:  
635 Acylating Agents in Organic Synthesis, *Chemical Reviews*, 119, 7113–7278,  
636 <https://doi.org/10.1021/acs.chemrev.8b00782>, 2019.
- 637 van Pinxteren, M., Müller, C., Iinuma, Y., Stolle, C., and Herrmann, H.: Chemical  
638 Characterization of Dissolved Organic Compounds from Coastal Sea Surface Microlayers  
639 (Baltic Sea, Germany), *Environmental Science & Technology*, 46, 10455–10462,  
640 <https://doi.org/10.1021/es204492b>, 2012.



- 641 van Pinxteren, M., Zeppenfeld, S., Fomba, K. W., Triesch, N., Frka, S., and Herrmann, H.:  
642 Amino acids, carbohydrates, and lipids in the tropical oligotrophic Atlantic Ocean: sea-to-air  
643 transfer and atmospheric in situ formation, *Atmospheric Chemistry and Physics*, 23, 6571–6590,  
644 <https://doi.org/10.5194/acp-23-6571-2023>, 2023.
- 645 Rachmilovich-Calis, S., Masarwa, A., Meyerstein, N., Meyerstein, D., and van Eldik, R.: New  
646 Mechanistic Aspects of the Fenton Reaction, *Chemistry – A European Journal*, 15, 8303–8309,  
647 <https://doi.org/10.1002/chem.200802572>, 2009.
- 648 Renard, P., Brissy, M., Rossi, F., Leremboure, M., Jaber, S., Baray, J.-L., Bianco, A., Delort,  
649 A.-M., and Deguillaume, L.: Free amino acid quantification in cloud water at the Puy de Dôme  
650 station (France), *Atmospheric Chemistry and Physics*, 22, 2467–2486,  
651 <https://doi.org/10.5194/acp-22-2467-2022>, 2022.
- 652 Samavat, S., Gholami, N., and Nazari, K.: Complexation of Iron (III) With Citrate and Tartarate  
653 Anions in Perturbed Aqueous Solutions Using Potentiometry and Difference UV/Vis. and IR  
654 Spectrophotometric Methods., *Acta Chimica Slovenica*, 54, 2007.
- 655 Samy, S., Robinson, J., and Hays, M. D.: An advanced LC-MS (Q-TOF) technique for the  
656 detection of amino acids in atmospheric aerosols, *Analytical and Bioanalytical Chemistry*, 401,  
657 3103–3113, <https://doi.org/10.1007/s00216-011-5238-2>, 2011.
- 658 Shulman, M. L., Charlson, R. J., and James Davis, E.: The effects of atmospheric organics on  
659 aqueous droplet evaporation, *Journal of Aerosol Science*, 28, 737–752,  
660 [https://doi.org/10.1016/S0021-8502\(96\)00469-7](https://doi.org/10.1016/S0021-8502(96)00469-7), 1997.
- 661 von Sonntag, C. and Schuchmann, H.-P.: The Elucidation of Peroxyl Radical Reactions in  
662 Aqueous Solution with the Help of Radiation-Chemical Methods, *Angewandte Chemie*  
663 *International Edition in English*, 30, 1229–1253, <https://doi.org/10.1002/anie.199112291>, 1991.
- 664 Soriano-Molina, P., García Sánchez, J. L., Alfano, O. M., Conte, L. O., Malato, S., and Sánchez  
665 Pérez, J. A.: Mechanistic modeling of solar photo-Fenton process with  $\text{Fe}^{3+}$ -EDDS at neutral  
666 pH, *Applied Catalysis B: Environmental*, 233, 234–242,  
667 <https://doi.org/10.1016/j.apcatb.2018.04.005>, 2018.
- 668 Sorooshian, A., Wang, Z., Coggon, M. M., Jonsson, H. H., and Ervens, B.: Observations of  
669 Sharp Oxalate Reductions in Stratocumulus Clouds at Variable Altitudes: Organic Acid and  
670 Metal Measurements During the 2011 E-PEACE Campaign, *Environmental Science &*  
671 *Technology*, 47, 7747–7756, <https://doi.org/10.1021/es4012383>, 2013.
- 672 Strathmann, T. J. and Stone, A. T.: Reduction of Oxamyl and Related Pesticides by  $\text{Fe}^{\text{II}}$ :  
673 Influence of Organic Ligands and Natural Organic Matter, *Environmental Science &*  
674 *Technology*, 36, 5172–5183, <https://doi.org/10.1021/es0205939>, 2002.
- 675 Sun, L., Wu, C.-H., and Faust, B. C.: Photochemical Redox Reactions of Inner-Sphere  
676 Copper(II)-Dicarboxylate Complexes: Effects of the Dicarboxylate Ligand Structure on  
677 Copper(I) Quantum Yields, *The Journal of Physical Chemistry A*, 102, 8664–8672,  
678 <https://doi.org/10.1021/jp982045g>, 1998.
- 679 Tilgner, A., Bräuer, P., Wolke, R., and Herrmann, H.: Modelling multiphase chemistry in  
680 deliquescent aerosols and clouds using CAPRAM3.0i, *Journal of Atmospheric Chemistry*, 70,  
681 221–256, <https://doi.org/10.1007/s10874-013-9267-4>, 2013.



- 682 Triesch, N., van Pinxteren, M., Salter, M., Stolle, C., Pereira, R., Zieger, P., and Herrmann, H.:  
683 Sea Spray Aerosol Chamber Study on Selective Transfer and Enrichment of Free and Combined  
684 Amino Acids, *ACS Earth and Space Chemistry*, 5, 1564–1574,  
685 <https://doi.org/10.1021/acsearthspacechem.1c00080>, 2021.
- 686 Wang, T. L., Tong, H. W., Yan, X. Y., Sheng, L. Q., Yang, J., and Liu, S. M.: Determination  
687 of Volatile Carbonyl Compounds in Cigarette Smoke by LC-DAD, *Chromatographia*, 62, 631–  
688 636, <https://doi.org/10.1365/s10337-005-0675-8>, 2005.
- 689 Wang, Z., Chen, X., Ji, H., Ma, W., Chen, C., and Zhao, J.: Photochemical Cycling of Iron  
690 Mediated by Dicarboxylates: Special Effect of Malonate, *Environmental Science &*  
691 *Technology*, 44, 263–268, <https://doi.org/10.1021/es901956x>, 2010.
- 692 Weller, C., Horn, S., and Herrmann, H.: Photolysis of Fe(III) carboxylato complexes: Fe(II)  
693 quantum yields and reaction mechanisms, *Journal of Photochemistry and Photobiology A:*  
694 *Chemistry*, 268, 24–36, <https://doi.org/10.1016/j.jphotochem.2013.06.022>, 2013.
- 695 Yuan, Y., Feng, L., Xie, N., Zhang, L., and Gong, J.: Rapid photochemical decomposition of  
696 perfluorooctanoic acid mediated by a comprehensive effect of nitrogen dioxide radicals and  
697  $\text{Fe}^{3+}/\text{Fe}^{2+}$  redox cycle, *Journal of Hazardous Materials*, 388, 121730,  
698 <https://doi.org/10.1016/j.jhazmat.2019.121730>, 2020.
- 699